A theoretical investigation on the effect of exhaust gas recycle versus excess air on spark-ignition engine performance

A.A. Hassan, M.M. El-Kassaby, M.M. Osman, and M.A. Hanafy
Mechanical Eng. Dept., Faculty of Eng., Alexandria University, Alexandria 21544, Egypt

A computer simulation of a four-stroke, spark-ignition engine thermodynamic cycle is presented. The simulation is based on the mass and energy conservation principles and the combustion process is simulated using two-zone combustion modeling. A kinetic model based on the extended Zeldovich mechanism is presented to predict the behavior of the variation of NO concentration during the combustion and expansion processes. The performance results predicted by the present simulation model are validated and found to be in good agreement with performance results found in literature. Comparison between the effects of Exhaust Gas Recycle (EGR) and air, as diluents in the inlet mixture, on NO engine emissions and engine performance has been investigated. Also, the effect of inlet EGR temperature variation on NO emissions was studied at different engine loads and speeds.

فى هذا البحث، تم إنشاء نموذج ثرمويناميكي لمحرك بنزين رباعى الأشواط باستخدام برمجة الحاسب الآلي. النموذج الثرموينـاميكي تم بنائـه باستخدام قانون بقاء الكتلة والقانون الأول للديناميكا الحرارية وقد تم تقسيم محتويات عملية الحريق إلى منطقتين، منطقة الخليط الغير محترق ومنطقة الغازات المحترقة. تم أيضا استخدام نموذج كيناتيكى لحساب أكسيد النيتروجين داخل الأسطوانة خلال عملية الاحتراق وعملية التمدد. تم التأكد من صحة النموذج الثرموديناميكي من خلال مقارنة النتائج التى تم استنتاجها من النموذج المقدم بنتائج معملية أجريت على محرك بنزين أحادى الأسطوانة، بالإضافة إلى ذلك تم مقارنة النتائج التى تم استنتاجها من النموذج المقدم بنتائج نموذج ثرموديناميكى آخر باستخدام مواصفات محرك ذو ثمانية اسطوانات. فى كلا المقارنتين كان هناك توافقا جيدا بين النتائج مما يعطى الثقة على أن النموذج الثرموديناميكي المقدم بنائـه بصورة صحيحة. تم استخدام النموذج الثرموديناميكي المقدم لدراسة أداء محرك البنزين حيث تم عقد مقارنة بين تأثير استخدام غازات العادم وتأثير الهواء، كإضافات لشحنة الهواء والوقود الأساسية، على انبعاثات أكسيد النيتروجين واستهلاك الوقود وفترة الحريق وضغط دخول الشحنة ومتوسط درجة حرارة غازات العادم والحرارة المفقودة بالتبريد، هذه المقارنة تمت دراستها عند حمل ثابت و قيم مختلفة لسرعات المحرك. تم أيضا دراسة تأثير تغير درجة حرارة غازات العادم التى يعاد تدويرها على انبعاثات أكسيد النيتروجين. كذلك تم دراسة تأثير إعادة تدوير غازات العادم على انبعاثات أكسيد النيتروجين واستهلاك الوقود وفترة الحريق وذلك عند أحمال وسرعات مختلفة للمحرك.

Keywords: Combustion, EGR, Modelling, SI engine, Thermodynamic

1. Introduction

Internal combustion engines are a major source of urban air pollution. The spark-ignition engine main pollutants include oxides of nitrogen, carbon monoxide CO, and organic compounds which are unburned or partially burned HydroCarbons (HC) [1]. Thus the most important objectives that the engine designer should satisfy is to develop engines with lower emissions and lower fuel consumption. However, fuel economy is sometimes sacrificed in order to meet NO_x emission limits by retarding the spark timing [2]. At part-load operating conditions, it is advantageous to dilute the fuel-air mixture. This is achieved either with excess air or with Exhaust Gas Recycle (EGR) which means introduction of a fraction of the engine exhaust gases back into the engine intake manifold through a control valve to dilute the charge going to the combustion chamber.

Lean burn and EGR are two commonly used techniques for improving fuel consumption and controlling emissions. Each has advantages and disadvantages when applied to an engine. To meet future emissions standards and economy fuel consumption requirements, most production engines are likely to use one or both techniques.

Patterson and Van Wylen [3] in 1964 reported one of the first thermodynamic simulations that included unburned and burned zones, heat transfer, and flame propagation for homogeneous charge engines. This simulation did not, however, include flow rates, heat transfer from the unburned zone, and other features. Nevertheless, this

simulation was a corner stone for a long history of the development and use of thermodynamic engine cycle simulations.
Heywood et al. [4] described one of the first simulations using three zones for the combustion process. In this simulation, the burned zone was divided into an adiabatic core and a boundary layer zone in addition to the unburned zone. The combustion duration was input to the simulation program. Heywood et al. studied the effect of the variations of load, speed, combustion duration, spark timing, equivalence ratio, EGR, and compression ratio on fuel consumption, NO emissions, and mean exhaust temperature. They found that at constant load, speed, equivalence ratio, and burn duration, the NO emissions, specific fuel consumption, and mean exhaust temperature all decrease with increasing EGR.

An experimental comparison between the effect of EGR and lean-burn on NO and HC exhaust emissions, brake specific fuel consumption, and combustion stability has been investigated by Lumsden et al. [5] in 1997. The study was performed at constant load and speed and stoichiometric mixture in the case of EGR. They found that EGR strategy gave excellent NO_x emissions control, an increase in HC emissions, and small but significant improvements in fuel economy, whereas the advantage of lean-burn is the relatively higher reduction in fuel consumption.

Bhargava et al. [6] studied experimentally the effect of EGR variations on engine emissions and thermal efficiency. The study was performed using 3.7 liter, lean-burn natural gas engine. Engine tests were performed at constant load and speed. They found that addition of EGR to an already lean operation, at constant air to fuel ratio, reduced oxides of nitrogen, but diluted the mixture to an extent that raised hydrocarbon emissions. Also, they found that thermal efficiency remains fairly constant with lower amounts of EGR and then rapidly decreases with increasing EGR.

A thermodynamic cycle simulation with three-zone combustion model was developed by Caton [7], in 2002, to predict performance, energy and availability characteristics for a production, 5.7liter, Spark-Ignition(SI) engine. In addition to the traditional formulations based on the first law of thermodynamics, the simulation also included considerations based on the second law of thermodynamics to calculate the entropy and availability during the engine cycle. Caton studied the effect of varying the compression ratio at constant load, speed, combustion period, and equivalence ratio on thermal efficiency. He also studied the effect of compression ratio and equivalence ratio variations on maximum cylinder gas temperature.

The objective of the present work is to describe a thermodynamic engine cycle simulation with two-zone combustion model for four-stroke cycle SI engine in order to study the effect of varying the amount of EGR and excess air in the inlet fresh mixture on engine performance and NO exhaust emissions. This achieved for simplicity by using the first principles such as the first law of thermodynamics, the ideal gas law, and treating the combustion process without using complicated relations and equations. Thus, the present model can represent a teaching and development tool for parametric studies of engine thermodynamics. What distinguishes the present model is its ability of calculating both the combustion duration and the start of combustion timing for MBT spark timing as a function of engine operating conditions and design parameters. In many previous similar simplified models such as the models constructed by Caton [7, 8], and Ferguson [9], the combustion duration was input as an assumed value. Although it is well known that accurate determination of NO emissions is restricted to multiple-zone combustion modelling, the two-zone combustion modelling could be used with sufficient accuracy for a qualitative determination of NO emission for predicting trends.

2. Model construction

For the present model, all cylinders of a multi-cylinder engine are assumed to be identical, to possess the same thermodynamic conditions, and to operate with identical conditions. Accordingly, this means that overall results for a multi-cylinder engine are

obtained by multiplying the results from the single cylinder analysis by the number of cylinders.

The following assumptions and approximations are considered for simplification:

1. The contents of the cylinder are fully mixed and spatially homogeneous in terms of composition and properties during intake, compression, expansion, and exhaust processes. Thus, the thermodynamic properties vary only with time (or crank angle).
2. For the combustion process, two zones (each is spatially homogeneous) are used. The two zones are the unburned and the burned zones. The two zones are separated from each other by the flame front (see fig. 2).
3. The intake and exhaust manifolds are assumed to be infinite plenums containing gases at constant temperature and pressure.
4. The flow rates in both the intake and exhaust processes are determined from quasi-steady one-dimensional flow rate equations.
5. All gases are considered to be ideal gases during the engine cycle.
6. The fuel (considered to be iso-octane) is assumed to be completely vaporized and mixed with the incoming charge.
7. Since only stoichiometric and lean mixtures are studied in the present work, the composition of EGR and residual gases is assumed to be a mixture of CO_2, H_2O, O_2, and N_2.
8. All crevice effects are ignored, and the blow-by is assumed to be zero.
9. The combustion efficiency is assumed to be 100% (i.e. no unburned fuel).
10. The cylinder walls temperature is assumed to be constant and the heat transfer is determined using Woschni correlation.
11. The engine is in steady state such that the thermodynamic state at the beginning of each thermodynamic cycle (two crankshaft revolutions) is the same as the end state of the cycle.

3. The thermodynamic formulation

Fig. 1 is a schematic of the engine cylinder, which shows cylinder heat transfer,

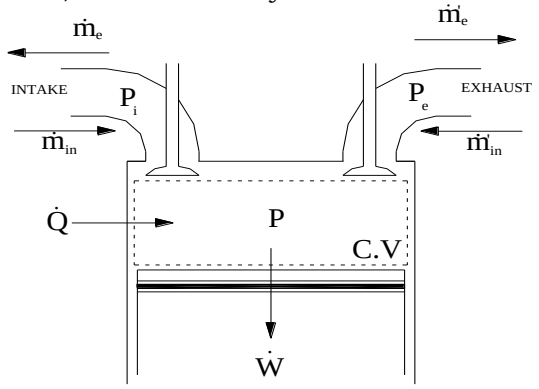

Fig. 1. Schematic of the thermodynamic control volume.

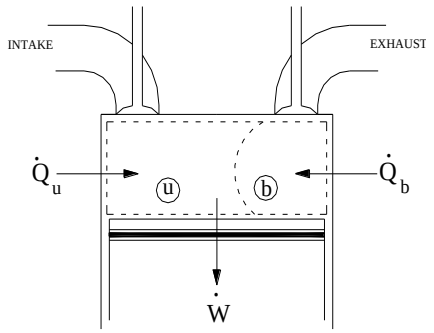

Fig. 2. Schematic of the two-zone combustion modeling.

work, and intake and exhaust flows during the valve overlap period. The basic relations used in the development of the present cycle simulation are the first law of thermodynamics, the conservation of mass law, and the ideal gas law.

These three important relations are applied to specified control volume, which will be always the cylinder volume, in order to derive expressions for the time (or crank angle) derivative of the gas temperature and pressure during engine processes. These expressions will be in terms of engine design parameters and operating conditions.

3.1. The gas exchange process

Due to the varying of valve open area and cylinder volume with time, gas inertia effects, and wave propagation in the intake and exhaust systems, the pressures in the intake and exhaust manifolds during gas exchange process vary in a complicated manner [1]. Since the present model is a detailed model of in-cylinder processes, then sophisticated intake and exhaust system models are not necessarily required, thus, the time-averaged

intake and exhaust manifold pressures are considered throughout the model formulation.

When the engine is throttled at part load, the back flow from the cylinder into the intake manifold occurs during the early part of the intake process until the cylinder pressure falls below the manifold pressure. Reverse flow can also occur in the compression stroke before the inlet valve closes, due to rising the cylinder pressure. When both intake and exhaust valves are open during overlap period, and when the inlet pressure is less than the exhaust pressure, back flow of exhausted gas into the cylinder will usually occur. This flow behavior is considered in the present model analysis when applying energy and mass conservation equations during the gas exchange process.

In the present model, the thermodynamic cycle simulation starts with assumed guesses of the values of pressure and temperature of the contents within the cylinder at the instant the intake valve opens. After two crankshaft revolutions (720 crank angle degrees), the calculated values of pressure and temperature are compared to the initial guesses. If the calculated values are not within an acceptable tolerance to the initial guesses, the simulation is repeated using the final calculated values as initial guesses. This procedure usually finds convergence within about 3 complete cycles.

During the intake process, the inlet charge is considered to be a mixture of air, vaporized fuel, and burned gases EGR entering the cylinder at uniform temperature and pressure during the intake process.

Applying the first law of thermodynamics for the control volume shown in fig. 1 during the intake process gives:

$$\dot{E}_{in} - \dot{E}_{out} = \frac{dE_{cv}}{dt} . \qquad (1)$$

Since the charge within the cylinder (the control volume), during the intake process, consists of a mixture of air, fuel vapor, EGR, and residual gases, then the internal energy of the contents within the cylinder can be written as:

$$E_{cv} = U_{cv} = m_{cv}u_{cv} = m_r u_r + m_{afe}u_{afe} . \qquad (2)$$

Then,

$$\frac{dE_{cv}}{dt} = \dot{m}_r u_r + m_r C_{v,r}\dot{T}_r + \dot{m}_{afe}u_{afe} + m_{afe}C_{v,afe}\dot{T}_{afe} . \qquad (3)$$

Where the subscript afe refers to the mixture of air, fuel, and EGR within the cylinder, whereas the subscript r refers to the cylinder residual gases retained from the previous cycle.

In the present model, the average temperature between the fresh charge within the cylinder and the residual gases is considered in the model analysis. Thus, a fully mixed charge is considered during the intake process, where it is assumed that each element of the fresh charge, which has just entered into the cylinder, mixes instantaneously with the contents of the cylinder which therefore have a uniform average temperature (i.e. $\dot{T}_r = \dot{T}_{afe} = \dot{T}$).

When inlet valve opens, the residual gases will either compressed or expanded to the inlet pressure depending upon whether the inlet pressure is greater or less than the exhaust pressure, which is close to the pressure of the residual gases. Thus, if inlet pressure is less than the exhaust pressure (as in the present work), the residual gases will flow into the intake manifold. Thus, part of the intake stroke will have to be used in returning these gases to the cylinder before fresh charge will enter into the cylinder.

Thus, $\dot{m}_r$ will be equal to zero during the main part of the intake process, and may have a value other than zero during the valve overlap period and during the early part of the compression stroke if back flow occurs.

$$\frac{dE_{cv}}{dt} = \dot{m}_r u_r + \dot{m}_{afe}u_{afe} + m_{cv}C_{v,cv}\dot{T} , \qquad (4)$$

$$m_{cv}C_{v,cv} = m_r C_{v,r} + m_{afe}C_{v,afe} . \qquad (5)$$

By substituting from the above relations into the first law of thermodynamics, the rate of change of cylinder temperature can be written as follows:

$$\dot{T} = \frac{\dot{Q} + \dot{m}_{in}h_{in} + \dot{m}'_{in}h'_{in} - p\dot{V} - \dot{m}_e h_e - \dot{m}'_e h'_e - \dot{m}_r u_r - \dot{m}_{afe}u_{afe}}{m_{cv}C_{v,cv}}. \quad (6)$$

Applying the ideal gas law for the cylinder contents:

$$pV = m_{cv}R_{cv}T . \quad (7)$$

By differentiating:

$$\dot{p} = \frac{\dot{m}_{cv}R_{cv}T + m_{cv}R_{cv}\dot{T} - p\dot{V}}{V} . \quad (8)$$

Eqs. (6 and 8) are used for calculating the instantaneous cylinder pressure and temperature during the intake process.

Since the cycle simulation starts with assumed values of pressure and temperature of the contents within the cylinder at the time the intake valve opens, then the initial mass of residual gases, $m_{r,i}$, can be calculated by applying the ideal gas law at the time the intake valve opens:

$$m_{r,i} = \frac{pV}{R_r T} . \quad (9)$$

The mass of residual gases at any instant within the cylinder, m_r, which changes during the valve overlap period and during any reverse flow, can be calculated as follows:

$$m_r = m_{r,i} + \sum(\dot{m}_{r,in} - \dot{m}_{r,out})\Delta t . \quad (10)$$

Where $\dot{m}_{r,in}$, and $\dot{m}_{r,out}$ are the flow rates of the residual gases entering and exiting the cylinder during a small period, Δt, respectively.

Similarly, the mass of the fresh charge (air, fuel, and EGR) at any instant within the cylinder, m_{afe}, can be calculated as follows:

$$m_{afe} = \sum(\dot{m}_{afe,in} - \dot{m}_{afe,out})\Delta t . \quad (11)$$

Where $\dot{m}_{afe,in}$, and $\dot{m}_{afe,out}$ are the flow rates of the fresh charge entering or exiting the cylinder during a small period, Δt, respectively.

Now, the total mass at any instant within the cylinder, m_{cv}, can be calculated as follows:

$$m_{cv} = m_r + m_{afe} . \quad (12)$$

Similarly, by applying the first law of thermodynamics and the ideal gas law during the exhaust process, the following two equations are deduced:

$$\dot{T} = \frac{\dot{Q} - p\dot{V} - \dot{m}'_e(h'_e - u_{cv})}{m_{cv}C_{v,cv}} , \quad (13)$$

$$\dot{p} = \frac{m_{cv}R_{cv}\dot{T} - p\dot{V} - \dot{m}'_e R_{cv}T}{V} . \quad (14)$$

Eqs. (13 and 14) are used for calculating the instantaneous cylinder pressure and temperature during the exhaust process.

3.2. The combustion process

Most of the two-zone engine combustion modelling techniques [1, 7, 9, and 10] are based on the following assumptions:

- The flame front thickness is assumed to be negligible.
- The cylinder pressure is assumed to be the same in the burned and unburned zones.
- Only the convective heat transfer mode, between the cylinder contents and the cylinder wall, is considered.
- The heat transfer between the two zones is neglected.
- For the burned zone, ten species (CO_2, H_2O, CO, N_2, O_2, OH, NO, H, O, and H_2) are considered in chemical equilibrium during combustion and expansion [9].
- The combustion chamber wall area in contact with the burned gases is assumed to be proportional to the square root of the burned mass fraction to account for the greater volume filled by burned gases as against the unburned volume.

In the present model, the thermodynamic analysis during combustion is based on applying the mass and energy conservation principles in addition to the ideal gas law for

each zone. Note that the properties of the burned zone are given a subscript (*b*), while the properties of the unburned zone are given a subscript (*u*).

Applying the first law of thermodynamics for the burned zone:

$$\dot{Q}_b + \dot{m}_b h_u - \dot{W}_b = \frac{d(m_b u_b)}{dt}, \quad (15)$$

where

$$\dot{Q}_b = h_{c,b} A_b (T_w - T_b). \quad (16)$$

$$\dot{W}_b = p \dot{V}_b. \quad (17)$$

Similarly, applying the first law of thermodynamics for the unburned zone:

$$\dot{Q}_u - \dot{m}_b h_u - \dot{W}_u = \frac{d(m_u u_u)}{dt}, \quad (18)$$

Where:

$$\dot{Q}_u = h_{c,u} A_u (T_w - T_u), \quad (19)$$

$$\dot{W}_u = p \dot{V}_u. \quad (20)$$

Applying the ideal gas law for the burned zone, and then differentiating:

$$\dot{p} V_b + p \dot{V}_b = \dot{m}_b R_b T_b + m_b R_b \dot{T}_b. \quad (21)$$

Applying the ideal gas law for the unburned zone, and then differentiating:

$$\dot{p} V_u + p \dot{V}_u = \dot{m}_u R_u T_u + m_u R_u \dot{T}_u, \quad (22)$$

Since:

$$V = V_b + V_u. \quad (23)$$

Then:

$$\dot{V} = \dot{V}_b + \dot{V}_u. \quad (24)$$

The above five eqs. (15, 18, 21, 22, and 24) are solved together in order to determine $\dot{p}$, $\dot{T}_u$, $\dot{T}_b$, $\dot{V}_b$, and $\dot{V}_u$ at any instant during combustion.

3.3. The burning rate

The S-shaped mass fraction burned profile is represented by Wiebe function as follows [1]:

$$X_b = 1 - exp\left[-a \left(\frac{\theta - \theta_o}{\Delta\theta} \right)^{m+1} \right]. \quad (25)$$

Where θ is the crank angle, θ_O is the crank angle at the start of combustion, $\Delta\theta_O$ is the total combustion duration (from X_b= 0 to X_b = 1), and a and m are adjustable parameters which fix the shape of the curve. Actual mass fraction burned curves have been fitted with $a \approx 5$, and $m \approx 2$ [1].

A combustion model has been used to obtain explicit relations for the flame development angle, $\Delta\theta_d$, and rapid burning angle, $\Delta\theta_b$, as functions of engine design and operating variables. These expressions show reasonable agreement with observed trends in both the flame development and rapid burning angles [1], and hence, these expressions are selected to be used in the present model in order to calculate the combustion duration ($\Delta\theta = \Delta\theta_d + \Delta\theta_b$) at different operating conditions. The combustion duration is then used to determine the burned mass fraction using Wiebe function.

The flame development angle was found [1] to vary as:

$$\Delta\theta_d = C (\bar{S}_p \nu)^{1/3} \left(\frac{h}{S_L} \right)^{2/3}, \quad (26)$$

Where ν is the kinematic viscosity ($\nu = \frac{\mu}{\rho}$), h is the distance between cylinder head and piston at ignition, S_L is the laminar burning velocity, $\bar{S}_p$ is the mean piston speed, and C is

a constant which depends on engine geometry and is determined by matching eq. (26) with engine data.

The rapid burn angle (here taken as the crank angle between X_b= 0.01and 1) is given by [1]:

$$\Delta\theta_b = C'\left(\frac{B}{h^*}\right)\left(\frac{\rho_i}{\rho_u^*}\right)^{10/9}\left(\bar{S}_p\, v^*\right)^{1/3}\left(\frac{h_i}{S_L^*}\right)^{2/3}. \quad (27)$$

Where C' is a constant which depends on engine geometry, ρ is the density, B is the cylinder bore, the subscript i denotes the value at ignition, and the superscript * denotes the value at cylinder conditions where X_b =0.5.

In the present model, the empirical rule for relating the mass burning profile to crank angle at MBT spark timing is used. With optimum spark timing, half the charge is burned at about 10 crank angle degrees after top dead centre [1]. Thus, referring to eq. (25), substituting X_b = *0.5* at θ = 730 degrees enables θ_o to be determined at specified combustion duration.

4. Kinetics of no formation

The mechanism of NO formation is described using the extended Zeldovich mechanism [1] .The rate of change of NO mole fraction during combustion and expansion can be calculated using the following relation:

$$\frac{dZ_{NO}}{dt} = \frac{2\, r_1\left(1-\left(Z_{NO}/Z_{NO,e}\right)^2\right)}{1+\left(Z_{NO}/Z_{NO,e}\right)r_1/(r_2+r_3)}, \quad (28)$$

where:

$$r_1 = k_1^+ \frac{P}{\bar{R}T_b} Z_{O,e}\, Z_{N_2,e}, \quad (29)$$

$$r_2 = k_2^- \frac{P}{\bar{R}T_b} Z_{NO,e}\, Z_{O,e}, \quad (30)$$

$$r_3 = k_3^- \frac{P}{\bar{R}T_b} Z_{NO,e}\, Z_{H,e}. \quad (31)$$

Where Z refers to mole fraction and the subscript e refers to equilibrium value.
The rate constants, in units of m^3/kmol.s, were calculated from ref. [1].

5. Results and discussion

A computer program using MATLAB computer programming software was developed based on the aforementioned model formulation. The simulation output is checked against results obtained from experiments on a Cooperative Fuels Research (CFR) single cylinder spark-ignition engine by LoRusso [11], with engine specifications shown in table 1.

The experimental results obtained by LoRusso [11] from the CFR engine operating at the conditions shown in table 2, which are compared to the present model predictions, were also used by Heywood et al. [4] in order to estimate their model validation.

Fig. 3 shows a comparison between the experimental *P-θ* curve and the matched calculated *P-θ* curve. Generally, there is a good agreement between the experimental and calculated pressure except for the maximum pressure. The quite difference between the calculated and the experimental cylinder pressure could be due to cycle to cycle

Table 1
CFR engine specifications, [11]

Item	Value
Number of cylinders	1
Compression ratio	7
Bore (mm)	82.6
Stroke (mm)	114.3
Connecting rod length (mm)	254
Intake valve opens (CAD BTDC)	10
Intake valve closes (CAD ABDC)	34
Exhaust valve opens (CAD BBDC)	40
Exhaust valve closes (CAD ATDC)	15

Table 2
CFR engine operating conditions, [11]

Engine speed (rpm)	1600
Excess air factor	1.234
Spark Timing for MBT (CAD BTDC)	32
Air flow (g/min)	201.4
Inlet pressure (kPa)	53

experimental cylinder pressure fluctuations that are significant especially for SI engines. This quite difference could be also due to any

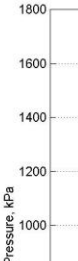

difference between the values of actual combustion parameters (such as combustion duration, start of combustion timing, etc) and the corresponding values used in the present simulation. Table 3 shows a comparison between calculated and measured performance parameters.

In order to study the effect of EGR on SI engine performance, a V-8 configuration, 5.7-liter displacement engine was chosen for this purpose. The engine geometry was based on Chevrolet 350 CID and Ford 351 CID engines which are closely comparable.

This engine was also used by Heywood et al. [4], and Caton [7, 8] in a set of related studies. Table 4 lists the engine specifications as provided by Heywood et al. [4] and as used in the present model. Predictions obtained by Caton model [7, 8] at the specified engine operating conditions, which are shown in table 5, were chosen to be compared with predictions obtained from the present model at the same engine operating conditions.

Fig. 4 shows a comparison between the calculated cylinder pressure, which varies with cylinder volume, as predicted by the present model and as predicted by Caton [8]. fig. 5 shows the temperature of the unburned mixture within the unburned zone, T_u, the temperature of burned gases within the burned zone, T_b, and the average cylinder contents temperature, T_{avg}, as functions of crank angle during combustion as predicted by the present model and as predicted by Caton [7].

Table 6 compares the major output parameters as predicted by the present model with those predicted by Caton [7, 8]. The global engine performance parameters such as power, mean effective pressure, thermal efficiency, and air and fuel flow rates are in very good agreement with the corresponding values calculated by Caton [7, 8].

In the light of the previous comparisons, it can be seen that there is, generally, a good agreement between the results in each comparison which implies that the present model is correctly developed and implemented.

Fig. 3. A comparison between the experimental pressure data [11] and the calculated pressure as predicted by the present model for 1600 rpm and 53 kPa inlet pressure.

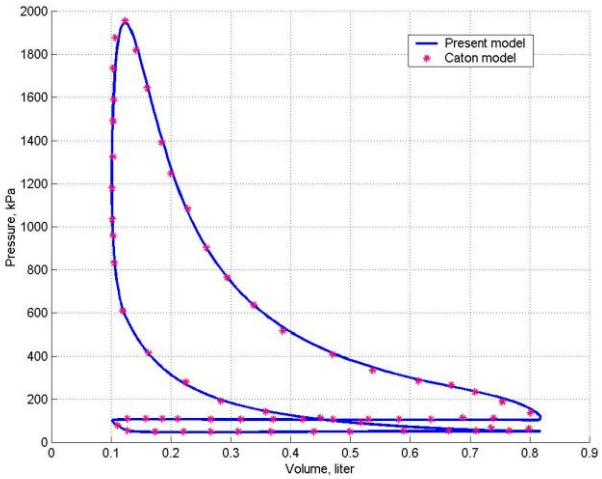

Fig. 4. A comparison between the calculated cylinder pressure as predicted by the present model and as predicted by Caton [8] at 1400 rpm and inlet pressure of 52 kPa.

Table 3
Comparison between calculated and measured performance parameters

Parameter	Experimental	Calculated	% Error
Air flow (g/min)	201.4	207.48	3
Gross imep (kPa)	367	367.5	0.14
Gross isfc (g/kW. h)	216	222.1	2.8

Table 4 Engine specifications, [4]

Number of cylinders	8
Compression ratio	8.1
Bore (mm)	101.6
Stroke (mm)	88.4
Crank radius to connecting rod length ratio	0.305
Intake valve opens (CAD BTDC)	14
Intake valve closes (CAD ABDC)	64
Exhaust valve opens (CAD BBDC)	64
Exhaust valve closes (CAD ATDC)	26

Table 5
Engine input parameters, [7, 8]

Engine speed (rpm)	1400
Excess air factor	1
Inlet manifold pressure (kPa)	52
Inlet charge temperature (K)	319
Exhaust manifold pressure (kPa)	105
% EGR	0
Combustion duration (CAD)	60
Start of combustion , θ_0 (CAD BTDC)	22

5.1. The effect of excess air variation on engine performance at different speeds

This performance study was investigated at net imep of 400 kPa (about 43% of the maximum load), and different engine speeds. Other operating conditions are: zero EGR, inlet charge temperature equals to 319 K, and MBT spark timing, and the inlet manifold pressure was varied for each excess air factor variation until the net imep of 400 kPa (with a tolerance within ±1kPa) is satisfied. The exhaust pressure variation with engine speed and inlet pressure was adapted from ref. [1].

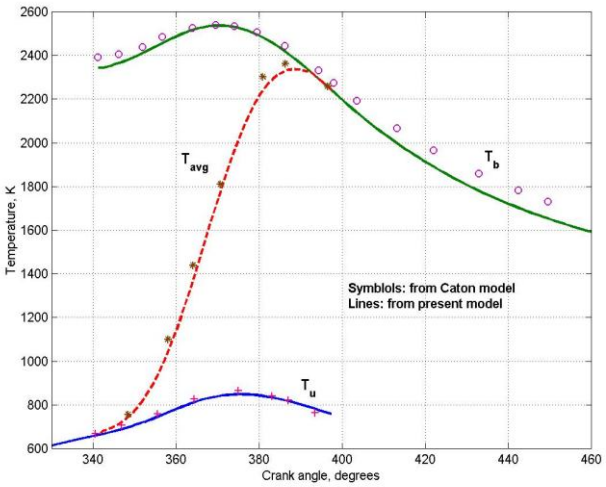

Fig. 5. Variations of unburned mixture temperature, burned gas temperature, and average cylinder contents temperature, during combustion as predicted by the present model and as predicted by Caton [7].

Fig. 6 shows the effect of excess air factor, λ, variation on net indicated fuel conversion efficiency at net imep of 400 kPa and three different engine speeds of 1400, 2000, and 3000 rpm (since the combustion efficiency was assumed to be 100%, then thermal efficiency has the same value as fuel conversion efficiency). The efficiency increases with increasing excess air up to a relatively high value of λ is reached. This increase can be attributed to the following three reasons:

1. Combustion of mixtures leaner than stoichiometric produces products at lower temperature, and with less dissociation of the molecules of CO_2 and H2O. Thus the fraction of the chemical energy of the fuel which is released as sensible energy near Top Dead Center (TDC) is greater, hence a greater fraction of the fuel energy is transferred as work to the piston during expansion, and the fraction of the fuel energy rejected to exhaust system decreases.
2. The heat loss to the cylinder walls is reduced because the temperature of burned gases is decreased (see table 7).
3. The pumping friction power is reduced with increasing λ, since the inlet pressure is increased with increasing excess air to maintain the load constant.

At the higher values of λ, the efficiency starts to decrease and continues decreasing with increasing λ. This is due to the increase in the burn duration, $\Delta\theta$, with increasing excess air. As the combustion duration increases, the combustion starts earlier, and hence, the compression work increases, also the combustion ends latter in the expansion stroke, and hence most of the fuel energy is converted to sensible energy far below TDC, which leads to expansion work decrease. Also, this increase in combustion duration indicates the practical possibility of partial burning or even misfire that could occur at high levels of air dilution.

As it can be noted from fig. 6, the value of λ at which the maximum efficiency is reached decreases with increasing engine speed. This is due to the increase in combustion duration in crank angle degrees with increasing engine speed.

Table 6
A Comparison between performance results as predicted by present model and caton [7,8].

Item	Caton [7,8]	Present model	% Error
Net indicated power (kW)	26.9	27.136	0.9
Net imep (kPa)	401.9	405.68	0.9
Net indicated thermal efficiency (%)	30.8	31.138	1.1
Air flow rate, (g/s)	29.68	29.7	0
Fuel flow rate (g/s)	1.97	1.963	0.35
Maximum cylinder pressure (kPa)	1955	1948	0.36
Crank angle of P_{max} (CAD ATDC)	17.1	17.2	0.58
Maximum T_b (K)	2545	2538	0.28
Crank angle of $T_{b,max}$ (CAD ATDC)	10.1	10.2	1

Table 7
Variations of maximum burned gases temperature, mean exhaust temperature, heat loss, inlet pressure, and pumping friction mean effective pressure with λ at net imep of 400 kpa and 1400 rpm

λ	1	1.1	1.2	1.3	1.4	1.5
$T_{b,max}$ (K)	2535	2467	2380	2296	2224	2171
$\overline{T}_{ex}$ (K)	1197.7	1164.7	1123.2	1082.8	1048.3	1019.9
$\dot{Q}$ (kW)	19.13	18.65	18.07	17.53	17.18	17.1
P_i (kPa)	51.6	54	56.9	60.05	63.65	67.75
pfmep (kPa)	57	54.7	52.4	49.6	46.3	43.18

The efficiency at engine speed of 2000 rpm is slightly higher than the efficiency at engine speed of 1400 rpm until about $\lambda \approx 1.25$. This is due to the decreased importance of heat transfer per cycle with increase of engine speed, whereas at the higher values of λ (high dilution), the effect of increasing the combustion duration with engine speed dominates. For relatively higher engine speeds, the efficiency is substantially lower due to the increase in both the pumping friction power and combustion duration that has a greater effect for leaner mixtures.

For NO calculation using the kinetic model, fig. 7 shows the effect of excess air on NO concentration at the end of expansion process. The maximum NO concentration is obtained at leaner mixtures than stoichiometric. This is due to the NO formation mechanism being a balance between oxygen availability and temperature. Peak burned gases temperature occurs in richer mixtures than stoichiometric, however the availability of oxygen means that the maximum NO formation occurs at slightly lean than stoichiometry. Once the NO peak has been passed, further additional air reduces the burned gas temperature and NO concentration is reduced.

5.2. The effect of %EGR variation on engine performance at different speeds

This engine performance study was investigated at net imep of 400 kPa, and different engine speeds. Other operating conditions are stoichiometric mixture, inlet fuel-air mixture temperature = 319 K, inlet recycled exhaust gases temperature = 1000 K, and MBT spark timing. The inlet manifold pressure was varied for each %EGR variation until the net imep of 400 kPa (with a tolerance within $\pm$ 1kP$_a$) is satisfied.

Fig. 8 shows the effect of %EGR in the inlet mixture variations on net indicated fuel conversion efficiency. For the relatively lower values of %EGR in the inlet mixture, the efficiency increases with increasing %EGR at all engine speeds. This is due to the reduction in degree of dissociation in the high temperature burned gases, because the burned gases temperature decreases with increasing the percentage of EGR in the inlet mixture, which allows more of the fuel chemical energy to be converted to sensible energy near TDC. Also, the pumping friction power (as it is calculated by the present model) decreases with increasing %EGR since the inlet pressure is increased with increasing %EGR to maintain the load constant with 400

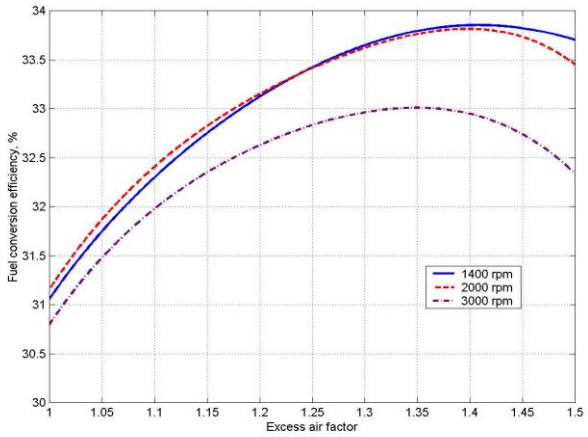

Fig. 6. Variation of net indicated fuel conversion efficiency with excess air factor at net imep of 400 kPa and different engine speeds.

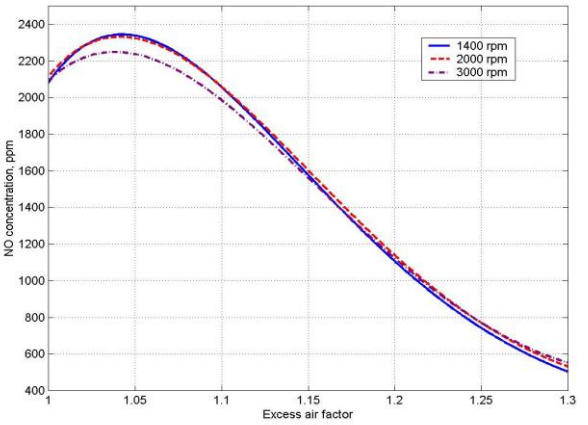

Fig. 7. Variation of NO concentration at the end of expansion process with excess air factor at net imep of 400 kPa and different engine speeds.

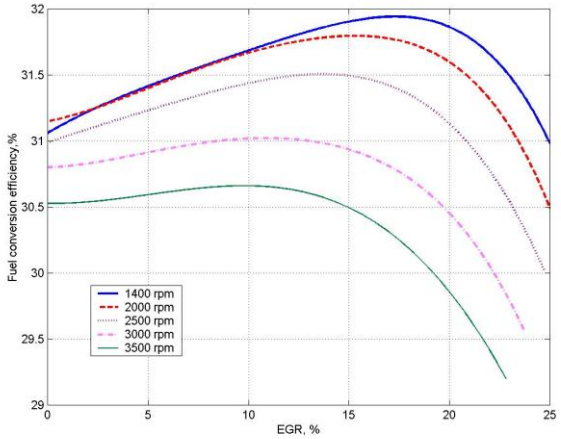

Fig. 8. Variation of net indicated fuel conversion efficiency with %EGR for stoichiometric mixture, net imep of 400 kPa, and different engine speeds.

kPa. With increasing %EGR, the temperature of burned gases is reduced, this temperature reduction is offset by the increase in combustion duration that necessitates early ignition during the compression stroke and a late end of combustion during the expansion stroke. For excessive charge dilution, the excessive increase in combustion duration slows down the combustion rate significantly, thus slightly more fuel is needed in order to burn an appropriate amount of fuel near TDC to maintain the load constant with 400 kPa. This increase in combustion duration with the consequent increased fuel consumption increases the heat loss and decreases efficiency.

Fig. 9 shows the effect of %EGR variation in the inlet mixture on NO concentration at the end of expansion process as predicted by the kinetic model. The admission of EGR increases the mass of the intake charge since the variations in both air and fuel flow rates are small. That results in lowering the combustion temperature since for the same almost net heat addition (from burning fuel) a greater mass of intake charge will result in a lower combustion temperature. Also, the greater specific heat capacity of EGR, due to the presence of carbon dioxide and water vapor, helps in reducing the combustion temperature. However, excessive charge dilution, which significantly slows down the combustion rate and increases the mass of fuel consumed would not be able to make any further reduction in cylinder temperature or NO emissions.

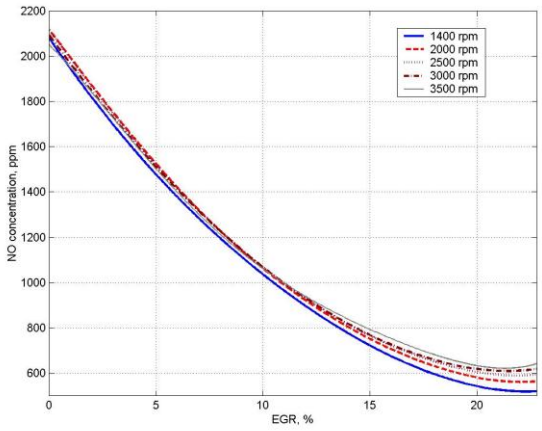

Fig. 9. Variation of NO concentration at the end of expansion process with %EGR for stoichiometric mixture, net imep of 400 kPa, and different engine speeds.

5.3. A comparison between the effect of excess air and EGR on engine performance

A comparison between the effects of air and EGR as diluents in the inlet mixture on engine performance was performed at 1400 rpm and net imep of 400 kPa.

Fig. 10 compares the effects of air and EGR as diluents on net indicated fuel conversion efficiency at 1400 rpm and net imep of 400 kPa. When EGR is used as diluent, the efficiency increases from 31.06% to maximum value of 31.95% at about %EGR=17, thus the percentage increase in efficiency is about 2.9%. When air is used as diluent the efficiency increases from 31.06% to about 33.25% at %Air dilution=17 with percentage increase in efficiency of 7.05%. However, the efficiency continues increasing with increasing air dilution until it reaches to about 33.8% at %Air dilution=25 with percentage increase in efficiency of 8.8%. From the previous discussion, it is noted that lean burn tends to achieve better fuel economy than EGR. This is due to EGR has a much greater effect on flame speed than air. Adding small amounts of EGR usually tends to increase the burn duration rapidly (as shown in fig. 12) to the point where the cycle efficiency starts to fall.

As it can be noted from fig. 12, high EGR dilution leaded to high values of the combustion duration. This high increase in combustion duration could lead to high cycle to cycle combustion variations, partial burning and even misfire, and hence, high HC emissions could be easily expected.

Fig. 11 compares the effects of air and EGR on NO concentration at the end of expansion process using the kinetic model. When EGR is used as diluent, NO emission is reduced by about 50% at %EGR=10, whereas there is no significant reduction in NO emission at the same percentage dilution in the case of air (%Air dilution=10). This is due to the availability of oxygen in the excess air, which encourages NO formation.

At high values of charge dilution with EGR, the rate of decrease of NO emission is reduced as a result of the significant increase of combustion duration and the consequent increase in fuel consumed, which affects the

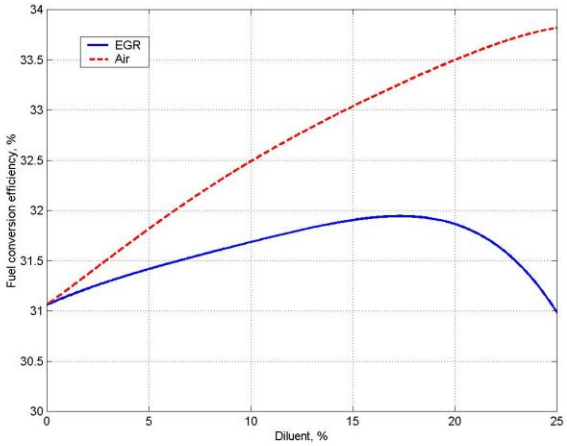

Fig. 10. A comparison between the effects of EGR and air on net indicated fuel conversion efficiency at net imep of 400 kPa and speed of 1400 rpm.

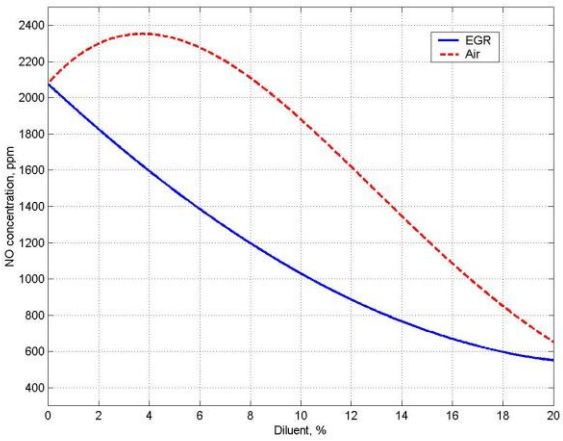

Fig. 11. A comparison between the effects of EGR and air on NO concentration at the end of expansion process at net imep of 400 kPa and speed of 1400 rpm.

trend of cylinder temperature decrease. Generally, EGR has a very significant effect on NO emission reduction as it can be noted from fig. 11.

5.4. The effect of EGR inlet temperature variation on NO emission

In the present model, a homogeneous inlet mixture (air, fuel, and EGR) with mass-average uniform temperature was assumed. In the previous performance studies, the inlet temperature of EGR was assumed to be 1000 K. It is advantageous to cool the burned gases (EGR), by using heat exchanger, before

entering to the engine cylinders. This cooling reduces the cylinder temperature, and hence, it reduces NO emission. Fig. 13 shows the effect of reducing the inlet EGR temperature from 1000 to 500 K on NO emission. As it can be noted from the figure, the reduction in NO emission is significant.

5.5. The effect of %EGR variation on engine performance at different loads

Performance studies similar to the ones obtained at net imep of 400 kPa are predicted at net imep of 500, 600, and 700 kPa for different engine speeds. These performance studies are done under the same engine operating conditions, which have been previously specified for the performance studies at 400 kPa and variable speeds.

Fig. 14 shows the variation of %EGR at which the maximum net indicated fuel conversion efficiency occurs with the engine load at different speeds.

For the load range under study (about 40% to 100% from the maximum load), %EGR at which the maximum efficiency occurs generally increases with increasing the engine load at constant speed until it reaches to a maximum value and then decreases to zero at WOT. This increase of %EGR is due to the decrease attained in the combustion duration with increasing the engine load (inlet pressure), which permits the engine to operate more efficient with more EGR. However, at higher engine loads, %EGR at which the maximum efficiency occurs represents the maximum %EGR the engine can accept to maintain the specified load constant, any further increase in EGR would decrease the fuel mass, and hence, the load. With faster burning rate combustion chambers, the engine could accept more EGR at higher loads and consequently would work more efficient.

For engine loads of about 40% to about 65% from the maximum load (maximum net imep), the percentage of EGR at which the maximum efficiency occurs depends mainly on the engine speed due to the increase of combustion duration with the increase of engine speed. For higher engine loads, %EGR at which the maximum efficiency occurs depends mainly on the engine load because adding further amounts of EGR at higher engine loads could decrease the fuel mass, and consequently, the load. Thus, %EGR at which the maximum efficiency occurs generally represents the maximum amount of %EGR that the engine can accept to maintain the specified high load constant, which will differ from engine to engine according to the design of combustion chamber and the combustion characteristics.

6. Conclusions

Based on the thermodynamic engine cycle simulation and the main results of the parametric studies, the following conclusions could be deduced:

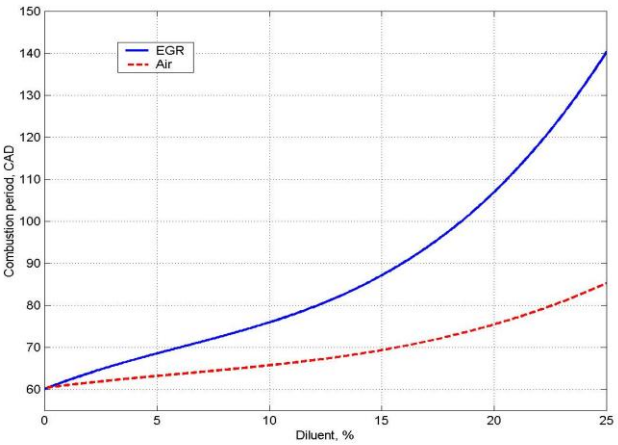

Fig. 12. A comparison between the effects of EGR and air on the combustion period at net imep of 400 kPa and speed of 1400 rpm.

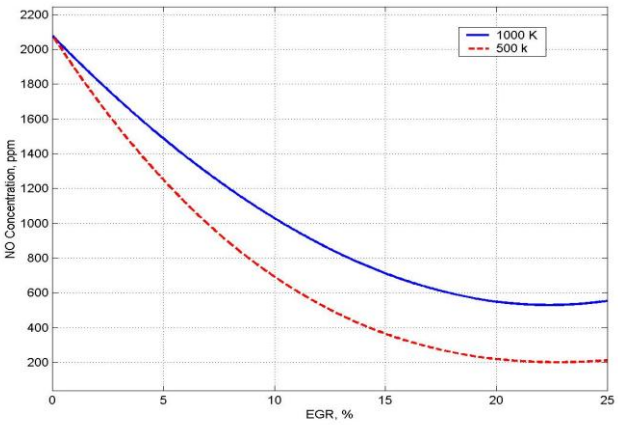

Fig. 13. The effect of inlet EGR temperature variation on NO concentration at the end of expansion process at net imep of 400 kPa and speed of 1400 rpm.

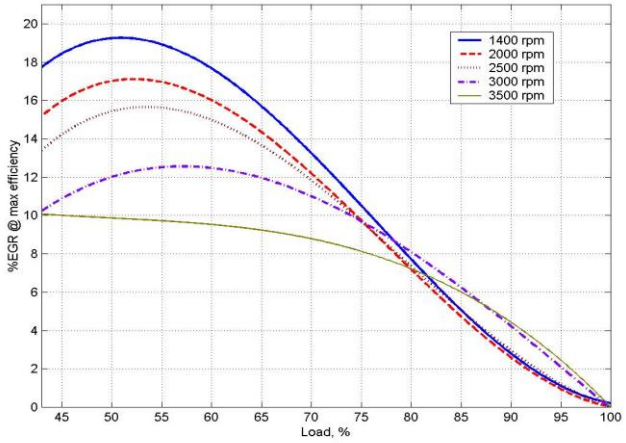

Fig. 14. Variation of %EGR at which the maximum net indicated fuel conversion efficiency occurs with the engine load at different speeds.

1. For a stoichiometric charge, moderate quantities of EGR showed excellent NO emissions control and slight improvements in fuel economy. The improvement in fuel economy was relatively significant at the lower engine speeds. Running with EGR also permits further exhaust after treatment using a three-way catalyst.
2. At the high level of EGR, the combustion rate substantially decreased, and consequently the fuel consumption started to increase rapidly especially at high engine speeds. Also, the rate of the decrease of NO emission was significantly reduced at the high level of EGR. The increase in HC emissions could be easily expected due to the slow combustion, and hence, partial burning, and even misfire that could occur at the high level of EGR.
3. Cooling of the exhaust-recycled gases (EGR) before entering the engine cylinders reduced the cylinder temperature, and hence, NO emissions.
4. The percentage of EGR at which the maximum engine thermal efficiency occurs depended mainly on engine speed for the load range of about 40% to 65% from the maximum load. However, at higher engine loads the percentage of EGR at which the maximum efficiency occurred depended mainly on engine load, which generally represented the maximum amount of EGR the engine could accept to maintain the specified load constant.
5. The advantage of lean burn was the very high significant improvement attained in the fuel economy. Unfortunately, lean burn predicted NO emissions higher than those achieved with stoichiometric mixture and EGR strategy, especially for the relatively lower inlet mixture dilution. In addition, using lean burn excludes the possibility of using a three-way catalyst.
6. To meet tighter NO emissions regulations, leaner operation (i.e., higher dilution) will be required. However, as the mixture is leaned the combustion rate decreases, and the increase in HC emissions could be expected.

Nomenclature

Symbols

A is the surface area,
V is the volume,
B is the cylinder bore,
W is the work,
E is the energy,
X_b is the burned mass fraction,
h is the specific enthalpy,
$\Delta\theta$ is the combustion duration,
h_c is the heat transfer coefficient,
$\Delta\theta_b$ is the rapid burning angle,
m is the mass,
$\Delta\theta_d$ is the flame development angle,
p is the pressure,
θ is the crank angle,
Q is the heat transfer,
θ_o is the start of combustion angle,
R is the gas constant,
λ is the excess air factor,
S_L is the laminar flame speed,
μ is the dynamic viscosity,
T is the temperature,
υ is the kinematic viscosity,
T_W is the wall temperature,
ρ is the density, and
U is the internal energy.

Abbreviations

ATDC After Top Dead Center,
EGR Exhaust Gases Recirculation,
BBDC Before Bottom Dead Center,
MBT Maximum Brake Torque,
CAD Crank Angle Degrees,

mep Mean Effective Pressure,
CFR Cooperative Fuels Research, and
WOT Wide Open Throttle.

References

[1] Heywood, B. John, "Internal Combustion Engine Fundamentals", McGraw-Hill Book Company, New York, ISBN 0-07-100499-8 (1988).

[2] R. Miller, G. Davis, G. Lavoie, C. Newman, and T. Gardner, "A Super-Extended Zeldovich Mechanism for NO_x Modeling and Engine Calibration", SAE Paper (980781) (1998).

[3] D.J. Patterson, and G. Van Wylen, "A Digital Computer Simulation for Spark-ignited Engine Cycles", Progress in Technology, Vol. 7 (1964).

[4] J.B. Heywood, J.M. Higgins, P.A. Watts, and R.J. Tabaczynski, "Development and Use of a Cycle Simulation to Predict SI Engine Efficiency and NO_x Emissions", SAE Paper (790291) (1979).

[5] G. Lumsden, D. Eddleston, and R. Sykes, "Comparing Lean Burn and EGR", SAE Paper (970505) 1997.

[6] S. Bhargava, N.N. Clark, and M.W. Hildebrand, "Exhaust Gas Recirculation in a Lean-Burn Natural Gas Engine", SAE Paper (981395) (1998).

[7] J.A. Caton, "A Cycle Simulation Including the Second Law of Thermodynamics for a Spark-Ignition Engine: Implications of the Use of Multiple Zones for Combustion", SAE Paper (2002-01-0007) (2002).

[8] J.A. Caton, "Comparisons of Instructional and Complete Versions of Thermodynamic Engine Cycle Simulations for SI Engines", International Journal of Mechanical Engineering Education, Vol. 29 (4) (2000).

[9] C.R. Ferguson, "Internal Combustion Engines ", John Willey and Sons, ISBN 0-471-83705-9 (1986).

[10] Y.G. Guezennec, W. and Hamama, "Two-Zone Heat Release Analysis of Combustion Data and Calibration of Heat Transfer Correlation in an Internal Combustion Engine", SAE Paper (999-01-0218) (1999).

[11] J.A. LoRusso, "Combustion and Emission Characteristic of Methanol, Methanol-Water, and Gasoline-Methanol Blends in a Spark-Ignition Engine", S. M. Thesis, Department of Mechanical Engineering, Massachusetts Institute of Technology (1976).

Received August 23, 2005
Accepted Fepruary 20, 2006